Instabilities and chaos in an infrared laser with saturable absorber: experiments and vibrorotational model

Ferdinando de Tomasi, Daniel Hennequin, Bruno Zambon, and Ennio Arimondo

Dipartimento di Fisica, Università di Pisa, Piazzo Torricelli, 2, 56100 Pisa, Italy

Received June 1, 1988; accepted July 27, 1988

The instabilities and chaos in a CO_2 laser containing SF_6 and $^{15}NH_3$ absorbers have been studied as a function of the laser-control parameters. By making use of a phase-portrait analysis, the instabilities have been classified through their orbits in the phase space around the laser-with-saturable-absorber (LSA) fixed points. A chaotic regime, reached through a sequence of period-doubling bifurcations, has been observed for an instability of limit cycles around one fixed point. The transition between different instability operations presents an intermediate regime, which we have defined as the hesitation regime and have characterized through the fluctuations in the return times. The observed phenomena have been reproduced within a model, including the rotational–vibrational structure of the amplifier and absorber media. The numerical analysis has shown that the LSA time evolution, as described through homoclinic orbits in the LSA phase space, depends on the relative attractions of the saddle point and the saddle focus fixed points.

1. INTRODUCTION

The observation of instabilities and chaos in nonlinear-optical systems is relevant for the operation of those systems and for the comprehension of quantum optics.[1] The optical nonlinearity of a laser with an intracavity saturable absorber (LSA) is associated with an absorber that operates in a regime of large saturation. The observation of instabilities as periodic modulations in the LSA output power goes back to the early operation of CO_2 laser in the aim of producing large pulses in the output power.[2] A fairly precise description of the LSA operation for CO_2 lasers containing intracavity molecular absorbers was given by Burak *et al.*[3] and by Dupré *et al.*,[4] with the rotational structure of the amplifier and absorber molecular media properly included in the rate equations of the so-called four-level model. By making use of the detailed semiclassical and quantized analyses of the LSA regimes by Lugiato *et al.*,[5] the threshold conditions for the cw and unstable regimes were determined in the frame of the four-level model.[6] Later, several authors investigated the LSA operation both experimentally and theoretically. Arimondo *et al.*[7] reported the observation of a LSA unstable regime with a sinusoidally modulated laser output power. Velarde and co-workers[8] and Mandel and co-workers[9] analyzed numerically in a few cases the solution of the LSA Maxwell–Bloch or rate equations in order to investigate output pulses and transitions between different regimes. The fluctuations in the laser intensity and return times in the pulsed regime have been investigated.[10,11] A different LSA model has been introduced by Tachikawa *et al.*[12] to describe the pumping process from the ground state of the CO_2 amplifier, producing a better description of the LSA pulses in the unstable regime. Finally, a chaotic regime in the LSA operation, theoretically predicted for unrealistic laser parameters, was recently observed experimentally.[13–15] The characterization of the LSA laser pulses in the unstable regimes through orbits in the phase space corresponding to homoclinic orbits, homoclinic cycles, and limit cycles has been discussed in Ref. 14. From the mathematical point of view the laser pulses in the homoclinic-orbit regime correspond to solutions emerging from a homoclinic solution through a so-called infinite-period bifurcation.[16,17]

CO_2 lasers belong to the so-called class-B lasers, for which an adiabatic elimination of the polarization may be performed and the laser operation is governed by two equations only. In fact, the unstable and chaotic features observed in the CO_2 LSA may be interpreted for the most part on the basis of the rate equations. Chaos has been observed in CO_2 lasers through an external manipulation of the laser dynamics, for instance, through laser modulation, injection of an external laser radiation, and feedback of the output intensity on the loss rate. Intrinsic chaos in CO_2 lasers has been observed by making use of a bidirectional ring cavity, i.e., in a system in which backward and forward field waves act as independent variables.[1] Chaos in the CO_2 LSA represents a new, important example of observation in intrinsic systems for which independent variables are associated with intrinsic quantities only.

The LSA system behaves differently from other autonomous or nonautonomous laser systems. Qualitatively the LSA phenomena are described through two rate equations for the amplifier and absorber media and an equation for the time evolution of the laser intensity. From that description the two fixed points in the phase space are determined, and the overall behavior of the LSA in both the unstable and the chaotic regimes may be interpreted on the basis of phase-space orbits around the two fixed points. However, the full complexity of the LSA regime is obtained when a more accurate modeling of the amplifier and absorber responses is introduced. In fact, the LSA systems encountered in the infrared experiments are described through a system with a larger number of equations in order to include the influence of the rotational coupling and the pumping from the ground state. This larger system leads to some new features in the LSA behavior. For instance, LSA systems show chaotic behavior through a sequence of period-doubling bifurca-

0740-3224/89/010045-13$02.00

tions. This chaotic behavior is related to the presence of a pumping mechanism in the amplifier medium. An important factor in LSA chaotic behavior is the occurrence, under appropriate conditions, of a Shil'nikov-type chaos, i.e., a motion characterized by homoclinic orbits in the phase space with large fluctuations in the return time associated with the sensitivity of the trajectory on the initial approach to the unstable point.[13] Such behavior, observed in a nonautonomous CO_2 system,[18,19] is characterized by a time evolution with pulses of constant amplitude but presenting fluctuations in their period. These chaotic regime results are quite different from those observed with period-doubling bifurcations. The LSA dynamics presents a saddle focus point with properties corresponding to those required for a Shil'nikov-type chaos. Our analysis of the LSA equation system, or more precisely the analysis of Shil'nikov's eigenvalues, shows that in correspondence to the experimental parameters, for the orbits diverging out from the second unstable point, the presence of a fixed point that is strongly attractive inhibits the chance of realizing a Shil'nikov chaos.

The aim of the present paper is twofold: to present a detailed experimental study of the LSA unstable and chaotic regimes and to perform a precise comparison between the experiment and the theoretical predictions when LSA is described through a model that includes the pumping from the ground state in the amplifier[12] and the four-level rotovibrational structure in the absorber.[6,20] In effect, on the basis of the model introduced in Ref. 12, Tachikawa *et al.*[21] have shown that the laser pulses in the unstable regime and the presence of the chaotic regime in the LSA operation are reproduced by using what they define as reasonable values for the laser parameters. Those parameters do not include the rotational structure in the low-pressure absorber and therefore are not appropriate for describing the LSA operation in the time-independent regimes, which are heavily affected by the rotational structure through the saturation intensity.[20] In the present paper we analyze how the absorber rotational coupling, which we have introduced into the LSA model, influences the chaotic regime, the instability windows, and the transitions between the different regimes.

This paper is organized as follows. In Section 2 a brief presentation of the laser and detection systems and a discussion of the LSA parameters are presented. In Section 3 the experimental results are reported. Modulated and chaotic output powers corresponding to different evolutions of the system inside the phase space are discussed, with state diagrams showing the different instability regimes as a function of the control parameters. In the LSA we have observed the presence of hesitations, i.e., the transitions between different regimes of instabilities present large fluctuations. We have explored the LSA hesitations through a return-time map and have characterized the orbit in the phase space by measuring the laser residence time around the fixed points.

The theoretical analysis, presented in Section 4, is based on the five-equation LSA model, including the rotational and vibrational complexities of the amplifier and absorber. We have explored numerically the solution of the LSA equations for parameters reproducing closely the static response of our system. The main results presented are the state diagrams of the LSA unstable and chaotic regimes and the characterization of the unstable points through their eigenvalues. Orbits in the phase space are used to characterize the LSA evolution and to introduce a classification of the different instability regimes.

Recently Dangoisse and Glorieux[22] analyzed the LSA chaotic regime within an ad hoc model for the amplifier and absorber media. That model may be derived from the more general one presented in this paper if an adiabatic elimination is applied to the absorber variables. It is remarkable that the oversimplified model of Dangoisse and Glorieux reproduces the main features of the chaotic dynamics, proving that the observed chaotic structures are entirely connected to the amplifier dynamics. In another recent analysis, Tanii *et al.*[23] examined the eigenvalues of the LSA system and their evolution as a function of the control parameters, with an aim similar to that of this paper, relating the LSA global behavior to the local eigenvalues.

2. EXPERIMENT

The LSA system and the data analysis were described previously.[20,24] It is relevant to the present description that the LSA system is characterized through the following parameters: A, defined as the ratio between the unsaturated amplifier gain and the cavity losses, $A = 1$ determining the laser threshold without the intracavity absorber; $\bar{A}$, defined as the ratio between the unsaturated absorption coefficient and the cavity losses; and a, defined as the ratio of the amplifier and absorber saturation intensities. In the dynamic regime, as well as in the static one, the laser evolution was monitored as a function of the pumping A parameter and the laser-frequency detuning Δ off the center frequency of the amplifier gain. However, the laser frequency affects all the A, $\bar{A}$, and a parameters through the amplifier and absorber detunings.

In the comparison between simulation and experimental results a precise knowledge of the laser parameters is required. The determination of the LSA parameters was based on (i) previous measurements, (ii) the comparison performed in Ref. 20 for the LSA static response, and (iii) the absorption coefficient and relaxation rates reported in the literature for the absorbing gases.

Our experimental observations were made by using SF_6 and $^{15}NH_3$ gases as saturable absorbers; their parameters are discussed in detail in Ref. 20. $^{15}NH_3$ presents the vibrational $aR(2, 0)$ transition in coincidence with the $10R(42)$ CO_2 laser line. SF_6 absorbs CO_2 laser radiation on several lines of the $10P$ branch, and in effect unstable and chaotic regimes were observed on nearly every laser line between $P(14)$ and $P(32)$. Bistable operations between the off, cw, unstable, and chaotic regimes have been observed on several lines. We report here results for the $P(20)$, $P(24)$, $P(30)$, and $P(32)$ lines.

For the laser-frequency detuning, the tuning center of the amplifier is easily determined. On the contrary, for the SF_6 experiments the position of the absorber line center cannot be determined precisely because for a few lines, for instance, $10P(16)$, the SF_6 absorption is composed of several lines spread around the CO_2 laser line center.[25] For other lines, for instance, $10P(30)$ and $10P(32)$, measurements of the frequency positions for the SF_6 absorption lines are not available.

A main problem encountered in the comparison between the theoretical analysis and the experimental results is that

most LSA experiments are performed in the regime of inhomogeneous broadening of the absorber transition line because a low-pressure absorber is introduced inside the laser cavity. Several observations were made by adding to the absorber a buffer gas, either He or CF_3Br, at a pressure of a few Torr in such a way that the results correspond to a regime with a homogeneously broadened absorber line.

3. RESULTS

A. Pulses and Phase Portraits

In analyzing the experimental observations of the unstable regimes in the LSA systems, it turns out that a large variety of regimes is obtained. To get some physics from the observations reported in this paper, as well as from the work reported previously in the literature, a sort of classification of the regimes is required. This classification is based on the results of our LSA theoretical analysis.

The overall LSA behavior is strongly determined by the presence of two fixed points in the phase space of the LSA variables. For the laser intensity, which is the variable usually observed in the experiment, these fixed points, defined as I_0 and I_+, are characterized, respectively, by a zero laser intensity and a laser intensity different from zero. The time evolution of the LSA is represented by an orbit in the phase space of the LSA variables winding around the two fixed points. Thus the classification of the LSA instabilities that we have introduced in Ref. 14 is based on the phase-space regions explored by the orbit.

The simplest and most common time-dependent regime for the LSA output power is composed of narrow spikes repeating regularly at a period T_p with constant amplitude. An example of that regime, which will be denoted as $P^{(0)}$, is shown in Fig. 1(a). The LSA system remains for a large part of the time T_p in a state corresponding to a zero laser intensity and for a narrow fraction of the period in states with output intensity different from zero. This $P^{(0)}$ regime may be described in the phase space through a quasi-homoclinic orbit, leaving the fixed point I_0 and reinjected into that point. If we limit our observation to the laser-intensity variable, the LSA system appears to evolve out of and into the zero-intensity state. On the contrary, the LSA is described through a full set of variables (at least four variables in the hypothesis of the most convenient adiabatic elimination), and even if the laser intensity has a zero value, we cannot determine from our experimental observations whether the LSA system remains near the I_0 point or simply in a phase-space region with zero laser intensity. Notice that if I_0 is a fixed point, a finite period phase-space trajectory cannot pass through that point, and a true homoclinic orbit occurs only at the bifurcation value for the instability regime,[26] i.e., at the so-called infinite-period bifurcation.[17]

If at fixed absorber parameters the pump parameter is increased, a region of unstable operation is realized when the single laser pulse on the laser output of Fig. 1 is followed by other pulses with smaller amplitudes. A typical result of this operation regime is presented in Fig. 2(a). To analyze the phase-space evolution over the LSA pulse, we have made use of a $[I(t), I(t+\tau)]$ phase-portrait representation, as shown in Fig. 2(b). It appears that the laser pulse corresponds to a trajectory evolving out of the I_0 saddle point and

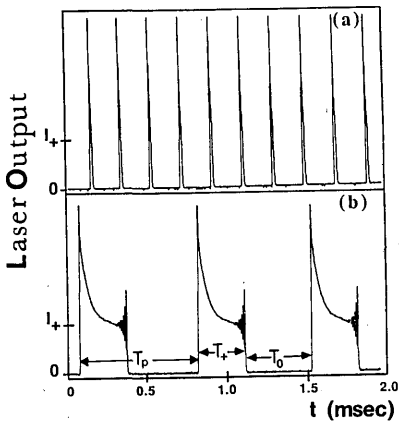

Fig. 1. (a) LSA output in a type-I $P^{(0)}$ instability corresponding to a quasi-homoclinic orbit in the phase space. (b) LSA output power in a type-I $\mathbf{P}^{(8)}$ instability corresponding to a quasi-homoclinic cycle in the phase space. Both instabilities were observed on the $10R(24)$ CO_2 amplifier at 25-mTorr SF_6 pressure with (a) $A = 1.03$ and (b) $A = 1.3$.

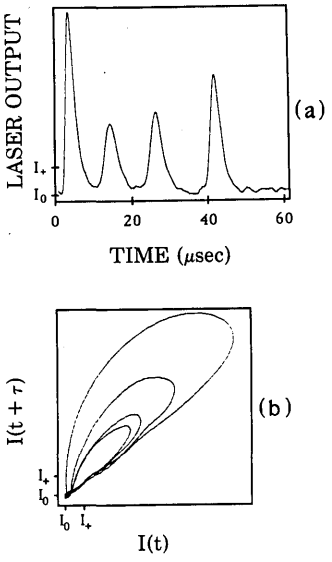

Fig. 2. (a) Laser pulse in a $P^{(3)}$ quasi-homoclinic instability revolving three times, after the initial main peak, out of I_0 and around I_+, as shown in the $I(t+\tau)$ versus $I(t)$ phase portrait presented in (b): $10P(32)$ CO_2 laser line at $A = 1.05$, SF_6:He in a 1:10 ratio, 200-mTorr total pressure, and $\tau = 0.6$ μsec.

orbiting around the saddle focus point I_+ before returning to the I_0 point. We have denoted the phase-space orbits in this regime as $P^{(n)}$, according to the number n of small-amplitude oscillations that the trajectory completes in the phase space around the saddle focus in between two successive long residences near the I_0 point. A similar definition for a similar regime has been introduced by Argoul *et al.*[27] in order to characterize the homoclinic chaos in the Belousov–Zhabotinskii reaction. The $P^{(n)}$ regimes correspond to quasi-homoclinic orbits leaving the I_0 point and reinjected into that point.

A different unstable LSA regime presents output pulses having high-frequency oscillations at the end of the pulse, as shown in Figs. 1(b) and 3(a). A phase portrait for those pulses is shown in Fig. 3(b). This regime, denoted as $\mathbf{P}^{(n)}$, is characterized by heteroclinic connections or homoclinic cy-

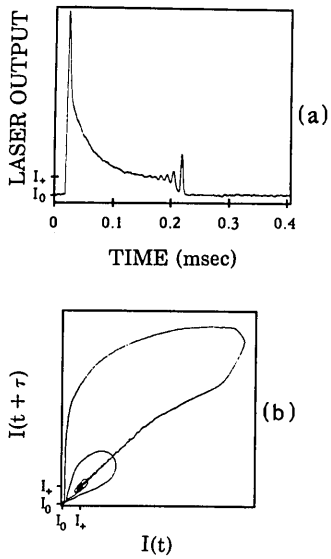

Fig. 3. As in Fig. 2 for a laser pulse in a $\mathbf{P}^{(5)}$ instability corresponding to a quasi-heteroclinic connection revolving out of I_0 into I_+ and later out of I_+ through five orbits: $10P(20)$ CO_2 line at $A = 1.3$, 20-mTorr SF_6 absorber pressure, and $\tau = 1$ μsec.

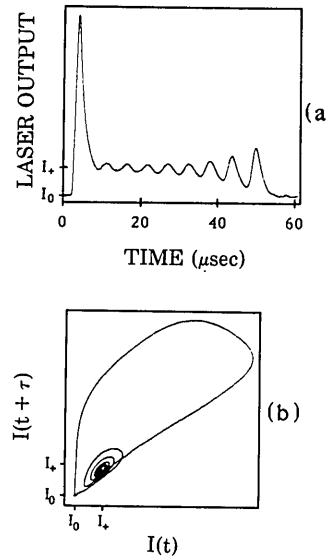

Fig. 4. As in Fig. 2 for a laser pulse in type-I instability corresponding to a regime intermediate between the homoclinic orbit and the heteroclinic connection: $10P(30)$ CO_2 line at $A = 1.1$, 40-mTorr SF_6 pressure, and $\tau = 0.6$ μsec.

cles,[26] in which the phase-space orbit leaving the area of I_0 at first converges toward the I_+ saddle focus, emerges from this point with a spiral-type motion, and finally is reinjected into the I_0 point.

If Figs. 2(a) and 3(a) represent two well-defined LSA regimes, then, by varying the laser-control parameters, laser pulses corresponding to intermediate regimes may be obtained; an example is shown in Fig. 4(a), and the phase portrait is shown in Fig. 4(b). In that case the phase-space orbit converges to the I_+ saddle focus and performs some small oscillations near but never reaches it. That LSA operation cannot be properly classified as a quasi-heteroclinic connection $\mathbf{P}^{(n)}$ regime and will still be denoted as $P^{(n)}$. Because the distinction between $\mathbf{P}^{(n)}$ and $P^{(n)}$ regimes appears as a fine-grain classification in respect to other LSA classification and a continuous transition occurs between them, the symbol $P^{(n)}$ will be used in what follows to denote all the intermediate regimes unless a specific reference is made to the occurrence of heteroclinic connections.

The LSA evolution in these instability regimes appears clearly in the three-dimensional representation of Fig. 5, as a function of the laser intensity I, the amplifier variable D, defined as the difference between the resonant vibrational-level populations, and the absorber variable $\bar{D}$, defined as the difference between the resonant rotational-level populations. Figure 5 was obtained from the numerical simulation of the LSA equations, and it will be discussed in Section 4. It is shown here to illustrate the support provided by the numerical simulation in the analysis and classification of the LSA pulses. This orbit, to be classified as $P^{(4)}$, approaches closely the I_+ point, as compared with other $P^{(n)}$ instabilities orbiting far from I_+. A phase-space trajectory reaches the I_+ point only in a homoclinic orbit or a heteroclinic connection at an infinite period bifurcation. The trajectory of Fig. 5 is distant from the I_0 point, with coordinates $(D_0, \bar{D}_0, 0)$, but the $I = I_0$ plane is an invariant surface from which the orbits arriving closely are repulsed.

All the $P^{(n)}$ regimes are characterized by the laser output power remaining for a large part of the T_p period in a state of zero laser intensity (see Fig. 1). Those pulses correspond to the regime well known as passive Q switching from the early days of CO_2 LSA operation[2] and were numerically analyzed by several authors (for instance, see Refs. 3 and 4). To separate this regime from the regime to be presented in Subsection 3.B, we denote it generically as a type-I instability.[14]

The laser output power may present another pulsed regime, which will be denoted type-II instability,[14] in which the laser intensity remains for most of the period around the intensity corresponding to the I_+ point. Thus small-amplitude oscillations near the I_+ intensity may appear on the

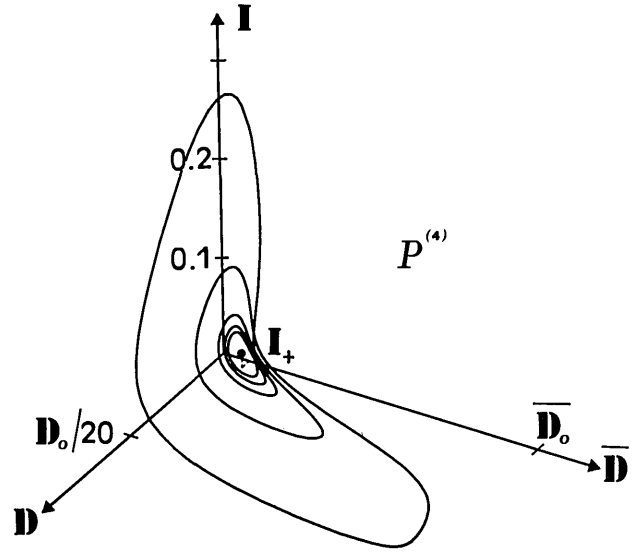

Fig. 5. Orbit in the three-dimensional phase space $(D, \bar{D}, I)$ as obtained from the numerical solution of the LSA equations. LSA parameters are as listed in Table 1 at $B_a = 25$ and $P = 1.74 \times 10^{-5}$.

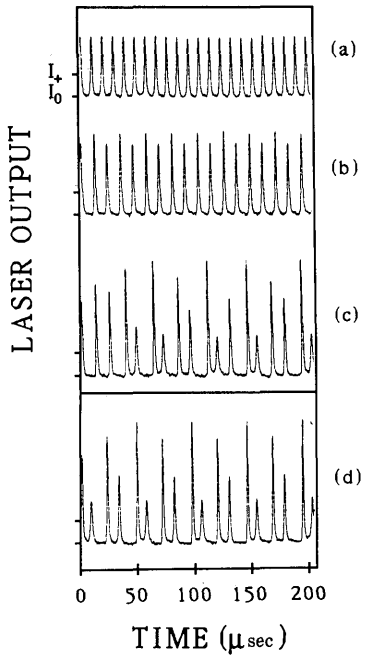

Fig. 6. (a) LSA output power in a type-II instability defined as a period T. (b) A bifurcation to a period $2T$ instability has been obtained. (c) A chaotic regime is observed, whereas in (d) a period doubling on $P^{(1)}$ is shown: $10P(32)$ amplifier, 70-mTorr SF_6 absorber, and 900-mTorr He buffer gas were used at (a) $A = 1.12$ and A reduced by 2% passing to (c), with laser frequency at center of the cavity mode. In (d) A is as in (b), and the laser frequency is detuned by 10 MHz. (The total phase diagram is given in Fig. 9.)

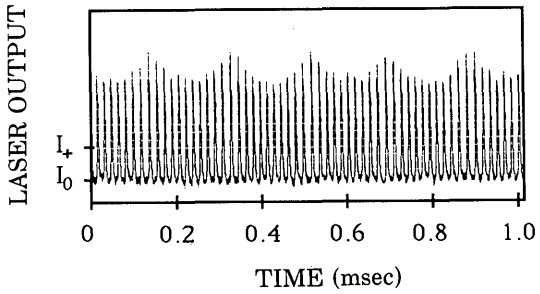

Fig. 7. Breathing oscillations observed on the LSA pulsed output power in a type-II instability: $10P(32)$ CO_2 laser operation and absorber SF_6 at 50 mTorr with 1-Torr He buffer gas.

LSA output power to be sinusoidal, as reported in Refs. 7 and 23, or with other shapes, as reported in Ref. 14. However, we are interested here mainly in pulses with large amplitude, as shown in Fig. 6(a). Notice that during the pulse the laser intensity passes through the zero-intensity value but only for a small fraction of the T_p period, and that makes the difference between the type-I and type-II instabilities. The regime with large-amplitude type-II pulses [Fig. 6(a)] will be denoted in what follows as the period-T regime. Phase-space orbits for type-II instabilities are presented by limit cycles around the saddle focus I_+, smaller or larger amplitudes depending on the specific pulses. Comparing Figs. 3 and 6, we notice that the period of the pulses in the T regime is close to the period of the oscillations spiraling out of the I_+ saddle focus. In fact, in both cases the period is approximately equal to the imaginary parts of the complex eigenvalues at the I_+ point.

Under some LSA operating conditions, the pulsed laser output shows a stable modulation of the self-pulsing envelope. A typical result for the period-T regime is shown in Fig. 7, and similar results have been observed for other LSA period-T operations. We have carefully checked that the low-frequency oscillations did not originate from fluctuations in the laser or detector power supplies. Furthermore, we noticed that the envelope modulation frequency varies regularly with pump parameter A. Thus the observed modulation envelope behavior may be interpreted as a breathing behavior, with the time scale of the breathing pattern 10–20 times longer than that of the self-pulsing oscillations. This slow periodic modulation of the period-T amplitude when represented in the phase space displays the characteristic behavior of a toroidal attraction around the I_+ saddle focus, as discussed in Ref. 27.

B. Chaos

Chaotic regimes were observed in our LSA system and were reached through a Feigenbaum scenario with a sequence of period doublings on type-II T instabilities. Experimental observations corresponding to that scenario are given in Fig. 6. A period-T regime shows a period-doubling bifurcation to an instability of period $2T$. Period-doubling bifurcations to regimes $4T$ and $8T$ have also been observed. Finally, a chaotic regime is reached. The data of Fig. 6 were obtained for a variation of the pump parameter A by 2% only.

In type-I instability a period-doubling bifurcation has been observed on the $P^{(1)}$ and $P^{(2)}$ regimes. An example of period doubling on the $P^{(1)}$, which will be denoted as $2P^{(1)}$, is represented in Fig. 6(d). However, no scenario to a chaotic regime has been observed within the type-I regime instability in our experiments on SF_6 or NH_3. In fact, in all the observed cases a transition to other regimes, typically type-II instabilities, has been obtained. On the contrary, the experimental observations of Ref. 13 with a CH_3I absorber have reported a route to chaos through period-doubling bifurcations on the $P^{(n)}$ regime. Thus in our experimental conditions such a route to chaos, if present, should occur within a narrow range of control parameters.

C. State Diagrams

We have investigated the occurrence of unstable and chaotic regimes in the LSA as a function of the laser-control parameters when different laser lines and absorbers were used. The convenient and most accessible control parameters are the A pump parameter and the amplifier detuning Δ, controlled through the cavity length. Notice that the cavity length modifies the amplifier detuning and the absorber frequency detuning at the same time. The evolution of the LSA regimes may be presented in a two-dimensional state diagram, with the pump and detuning parameters as coordinates. Two examples of experimentally determined state diagrams are shown in Figs. 8 and 9. Notice that the diagrams have been constructed by scanning both control parameters independently. In the figures we have used the pump parameter $A_0 = A(\Delta = 0)$ as obtained at the center of the cavity detuning. The laser output power depends on A_0 and the cavity detuning Δ.[14] Three types of evolution have been observed on the LSA operation as a function of one control parameter, for instance, increasing the discharge current at fixed laser frequency:

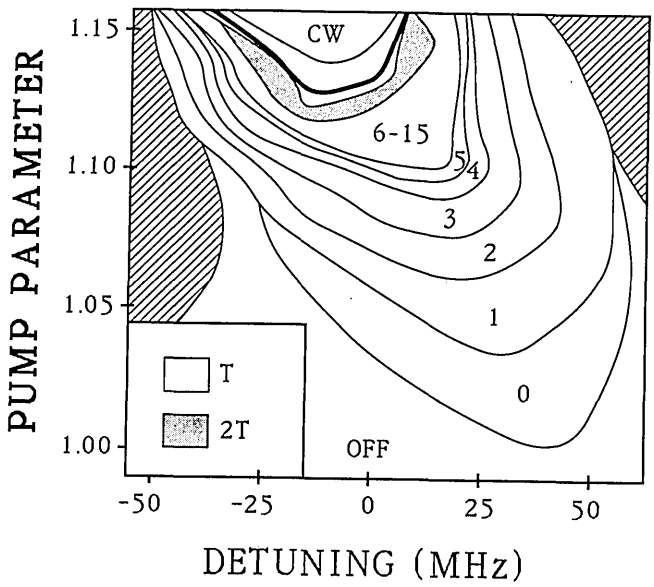

Fig. 8. LSA state diagram on the plane of the control parameters (A_0, Δ) for operation on the 10P(30) CO_2 line and 45-mTorr SF_6 pressure. In the hatched zones on the left- and right-hand sides of the diagram the laser is either multimode or on a different mode. An integer n denotes a region corresponding to a $P^{(n)}$ regime. The heavy line denotes the upper border of the type-I region. The regions near the cw operation correspond to T and $2T$ type-II unstable regimes. This diagram illustrates the bistability between type-I [here $P^{(8)}$ to $P^{(15)}$] and type-II unstable regimes (here T and $2T$).

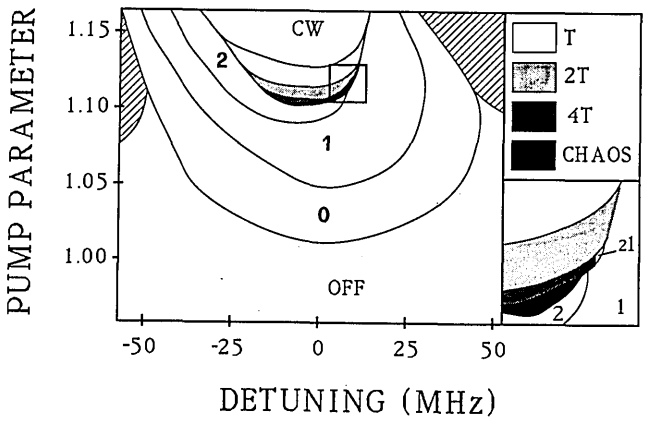

Fig. 9. LSA state diagram as in Fig. 8 for operation on 10P(32) line with 70-mTorr SF_6 absorber and 900-mTorr He buffer gas. The window in the lower right-hand corner is an enlargement of the region surrounded by the box in the center of the diagram. In this diagram the system presents within the region of type-II instabilities a Feigenbaum scenario with period-doubling cascades culminating in chaos. Outside that region the system presents a type-I passive Q-switching regime.

(1) Evolution from the off regime to a $P^{(n)}$ regime, first at small n numbers and later at large n numbers, with an evolution finally ending in a cw regime. Depending on the operating conditions, quasi-heteroclinic $\mathbf{P}^{(n)}$ cycles may appear in the evolution toward the cw regime, but, as pointed out above, at large n values the distinction between the $P^{(n)}$ and $\mathbf{P}^{(n)}$ regimes is minor. This evolution has been observed on all the laser lines between $P(22)$ and $P(28)$ with a low-pressure SF_6 absorber.

(2) Evolution from the off regime toward the $P^{(n)}$ regime and later at small n values, typically $n \sim 5$, with evolution into a chaotic regime associated with a supercritical type-II instability bifurcation series. When the control parameter is increased out of the chaotic regime, a type-II instability regime is reached through an inverse Feigenbaum sequence of period doublings, and finally the cw regime is obtained. This evolution was observed, for instance, on the 10P(32) laser line when a low-pressure SF_6 absorber and He buffer gas at a pressure ten times larger were used. The phase diagram of Fig. 9 presents clearly this possibility of LSA evolution when vertical lines are explored. Figure 9 shows regions with $P^{(1)}$ and $P^{(2)}$ regimes. Furthermore, the insert of Fig. 9 shows a small region of type-II period-doubling instabilities, identified as 21 in the figure.

(3) Evolution from the off regime into the $P^{(n)}$ unstable regime up to orbits with large n number ($n \sim 15$ in Fig. 8), without reaching a chaotic regime. On the contrary, the region of type-II instabilities is reached through a bistability between the type-I and type-II instabilities. The state diagram of Fig. 8 shows this overall evolution for 10P(32) CO_2 laser operation when SF_6 at 45-mTorr pressure was used. The bistability region is delimited above by the heavy line and below by the border of the period-doubling region.

Notice that the frequency detuning marked on the x axes of the figures represents the shift in the laser frequency produced by the modification in the cavity length in the absence of intracavity absorber. From the overall state diagrams of Figs. 8 and 9, we see that a frequency shift of the laser mode is produced by the absorber through a frequency pulling. Furthermore, we notice that the borderlines between the different regions of LSA operation depend on the laser alignment, and changes as great as 20% of the A and Δ values may be obtained by a slightly different laser alignment.

A main results of the state-diagram investigations is the observation of different cases of bistability in the LSA operation. The simplest and most obvious bistability occurs for LSA operation between cw and laser-off regimes. That appears, for instance, for 10P(16) CO_2 operation and a pure low-pressure SF_6 absorber at low-frequency detunings. When instabilities arise in the laser operation, bistabilities between type-I instability and the cw regime may appear, as observed in the operation with the 10P(20) line and low-pressure SF_6 absorber. On the contrary, for the 10P(16) line a bistability between type-II instability and the off regime has been observed. These observations indicate that in the LSA phase space an I_+ stable point and a stable type-I orbit coexist with an I_0 stable point and a stable type-II orbit. To complete the list, bistability occurs between an I_+ stable point and a type-II orbit, corresponding to the coexistence of a limit cycle around the I_+ point independent of the stable I_+ point itself. We have not obtained this bistable regime in our state-diagram reconstructions, but we have clear experimental evidence of it. A last observed bistability case is between type-I and type-II instabilities, and this case is illustrated in Fig. 8. In conclusion, only one case has not been obtained—bistability between I_0 and the type-I instability.

In passing between the various regimes, soft or hard transitions have been observed. Soft transitions are observed in the passage between the type-I unstable regime and the off

or cw regimes, i.e., the I_0 or I_+ stable points. In these soft transitions the period of the type-I instability diverges, corresponding to orbits emerging from a homoclinic solution. A hard transition is associated with the bistability between the off regime and cw regimes. Also, the transition between the off regime and the type-II instability appears to be associated with a bistability and thus to hard transition. The transition between the cw regime and the type-II instability appears to be either a soft or a hard transition, depending on the experimental conditions, proving that a limit cycle near I_+ may exist independently of the stable I_+ point leading to the cw regime. Similar behavior occurs for the transition between type-I and type-II instabilities, with soft transitions observed when the $P^{(n)}$ regimes at small n values are involved and hard transitions occurring for large n values. This proves that the two regimes are not similar even if the numerical analysis shows that it is possible to realize a continuous transformation of the orbits of one type into the orbits of another type.

D. Return Times and Hesitations

To characterize more precisely the different unstable or chaotic regimes of the LSA operation, we have investigated return times as a function of the laser-control parameters. In fact, return maps of the intensity and iteration map of the return time represent a standard approach to differentiating the regimes and also to distinguishing between an approach to the chaos through period-doubling bifurcations or Shil'nikov-type chaos.[18] In the LSA operation, with orbits visiting the I_0 and I_+ point, we have measured the time spent during the evolution in the phase space around each of these points. On the typical heteroclinic connection shown in Fig. 1(b) we have indicated the measured T_0 and T_+ times. T_0 represents the time spent during the LSA operation in the region of zero intensity. T_+ defines the time spent during the orbit around the I_+ point: it also includes the time spent along a large orbit in the phase space, but this time is a small fraction of the total T_+ time.

Figures 10 and 11 show experimental results for averaged $\langle T_0 \rangle$ and $\langle T_+ \rangle$ times as a function of the amplifier pump parameter for different conditions of LSA operation. Figure 10, for the operation on the $10R(42)$ laser line with a NH_3 absorber, refers to a heteroclinic instability at large n number. Figure 11, for the $10P(30)$ operation with a SF_6 absorber, corresponds to $P^{(n)}$ homoclinic instabilities at low n numbers. In both cases $\langle T_0 \rangle$ decreases with increasing pump parameter, and, in fact, $\langle T_0 \rangle$ diverges at the transition between the off (or cw) and pulsed operations, corresponding to a periodic solution emerging from a homoclinic solution (also called an infinite-period bifurcation[16,17,26]). On the contrary, $\langle T_+ \rangle$ increases with the pump parameter, and, in fact, $\langle T_+ \rangle$ diverges in passing from the pulsed to the cw regime. This behavior corresponds again to an infinite-period bifurcation, with a periodic solution emerging from a heteroclinic solution. The transition between different homoclinic instabilities in Fig. 11 takes place through a discontinuity in the T_+ time. An n-order homoclinic trajectory includes n windings around the I_+ point, and the T_+ time changes by a revolution around I_+ whenever the n index is modifed by one unit. That dependence of T_+ time appears at the intermediate pump amplifier parameter of Fig. 11(a) and, more specifically, in Fig. 11(b) for the transitions be-

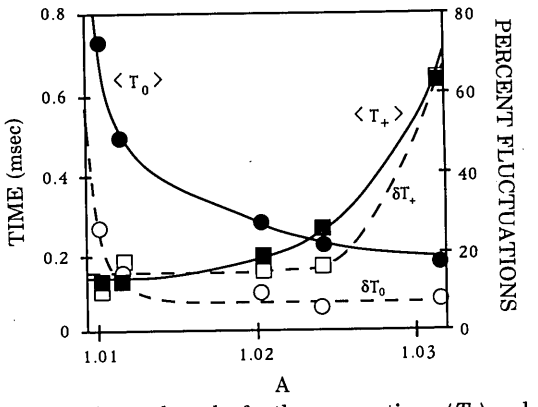

Fig. 10. Experimental results for the average times $\langle T_0 \rangle$ and $\langle T_+ \rangle$ and relative fluctuations δT_0 and δT_+ of those times as function of the A parameter for laser pulses corresponding to a quasi-heteroclinic connections: $10R(42)$ CO_2 laser line, 10-mTorr $^{15}NH_3$ absorber with 120-mTorr CF_3Br buffer gas. Notice that in this figure, as well as in Fig. 11, only a few experimental points have been drawn, and the continuous lines have been drawn through the experimental points.

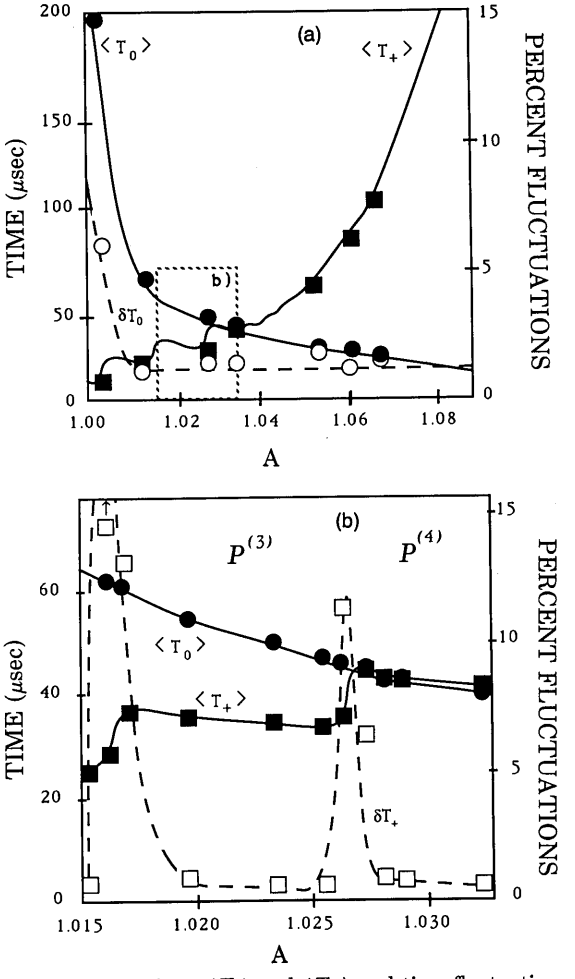

Fig. 11. Average times $\langle T_0 \rangle$ and $\langle T_+ \rangle$ and time fluctuations δT_0 and δT_+ as a function of the pump parameter A for the quasi-homoclinic instabilities on the $10P(30)$ laser line with 50-mTorr SF_6 pressure. (a) A global view; (b) on an enlarged scale, the region corresponding to the LSA transitions between the $P^{(2)}$ and $P^{(4)}$ regimes. The time fluctuations δT_+, not shown in (a) in order not to burden the figure, become large in the transition to the $P^{(2)}$ regime.

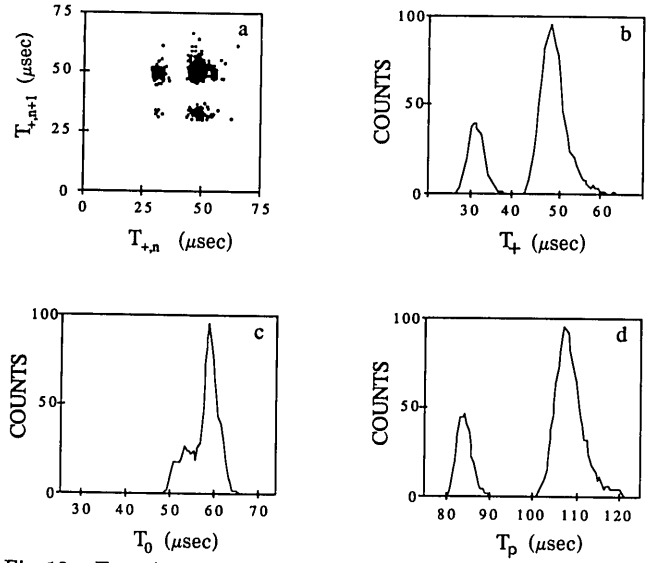

Fig. 12. Experimental results for the hesitations between $P^{(1)}$ and $P^{(2)}$ homoclinic instabilities on the 10P(30) line with 35-mTorr SF_6 absorber at $A = 1.02$. (a) Return-time map of the T_+ time. (b), (c), and (d) Distributions of the measured T_+, T_0, and T_p times, respectively.

tween the $P^{(2)}$–$P^{(3)}$–$P^{(4)}$ instabilities. Discontinuities in the T_+ time have not been noted for the heteroclinic trajectories corresponding to Fig. 10.

The measurements of the return times also point out the presence of hesitations for the LSA transitions between different regimes. In fact, the FWHM of the distribution in the return times has also been measured, and Figs. 10 and 11 show the FWHM as a percentage fluctuation of the averaged $\langle T_0 \rangle$ and $\langle T_+ \rangle$ times. It may be noticed that large fluctuations of the T_0 and T_+ times appear at the infinite period bifurcations. Moreover, large fluctuations in the T_+ times are observed in the transition between homoclinic instabilities. Figure 11(b) shows relative fluctuations in the T_+ time as great as 20% in the transition between the $P^{(2)}$ and $P^{(3)}$ regimes. The presence of discontinuity and large fluctuations in the T_+ times is described through hesitations of the LSA system between the different regimes. Thus, in a narrow region of LSA parameters, LSA hesitates in operation between trajectories with a different number of revolving orbits around I_+. The LSA hesitations may be linked either to stochastic mixtures of two adjoining periodic states produced by the influence of pump parameter noise on the LSA operation or to the existence of a narrow chaotic region located between different instability regimes. The above experimental observation does not allow us to distinguish between these different possibilities.

The iteration map of the return time is an appropriate indicator for the characterization of chaotic regimes. We have examined the return map of the T_+ times spent around the I_+ saddle focus point. Figure 12a shows an experimental return map of T_+ time in the hestitation between $P^{(1)}$ and $P^{(2)}$ regimes for LSA operation on the 10R(30) line with 35-mTorr SF_6 pressure. The T_+ time measured on the j pulse has been plotted versus the time T_+ measured on the $j-1$ pulse. The observed structure appears to be regular, with a broadening produced by the noise, as corresponding to a stochastic mixture between two different regimes. Thus the measured T_+ return map seems to exclude the presence of a chaotic regime.

Figures 12b–12d shows the distribution of the T_+ and T_0 return time and of the period T_p in the same conditions of hesitations between $P^{(1)}$ and $P^{(2)}$ as in Fig. 12a. Owing to the large fluctuation in the $P^{(1)}$–$P^{(2)}$ hesitation, the distributions of the T_+ and T_p times are double peaked, corresponding to a different number of revolutions around the I_+ point. On the contrary, the distribution of T_0 times remains single peaked, proving that the evolution near the I_0 point is independent of the evolution in the phase space around the I_+ point. The I_0 point produces a stabilizing action on the phase-space trajectory of the LSA.

4. THEORY

A. State Diagram

Within the model introduced in Ref. 17 and in the hypothesis of homogeneously broadened transitions, the CO_2 LSA response may be described on the basis of the following system of five equations:

$$
\begin{aligned}
dI/d\tau &= I(B_{sg}D - B_{sa}\bar{D} - 1),\\
dD/d\tau &= -2IB_gD - (R_{20} + R_{10} + 2R_{21})D/4k\\
&\quad - (R_{20} - R_{10} + 2R_{21} + 2P)S/4k + P/2k,\\
dS/d\tau &= -(R_{20} - R_{10})D/4k - (R_{20} + R_{10} + 2P)S/4k + P/2k,\\
d\bar{D}/d\tau &= -\gamma_R\bar{D} + \gamma'_R\bar{\Delta} - 2B_aI\bar{D},\\
d\bar{\Delta}/d\tau &= -\gamma'_R\bar{\Delta} + \gamma_R\bar{D} - \gamma_a(\bar{\Delta} - 1),
\end{aligned}
\tag{1}
$$

where $\tau = 2kt$ is the time measured in units of the inverse of the cavity loss $2k$. $D = M_2 - M_1$ is the difference between the amplifier vibrational-level populations, and S is their sum, with the total population of the three amplifier vibrational levels normalized to 1. P is the pumping rate from the ground state to the upper 2 level. $\bar{D}$ and $\bar{\Delta}$ are the absorber population differences between rotational and vibrational levels, respectively, normalized to the thermal equilibrium values, and I is the laser intensity. B_g, B_{sg}, B_a, and B_{sa} are coupling parameters between laser and amplifier and absorber media and R_{10}, R_{20}, R_{21}, γ, γ'_R, and γ_R are the relaxation rates defined in Refs. 6 and 12.

We have numerically solved the system of Eqs. (1) for the parameters corresponding to the LSA operation with SF_6 and $^{15}NH_3$ as saturable absorbers. However, the results presented here do not correspond precisely to any of those absorbers, and instead the slightly different LSA parameters introduced in the numerical analysis are such as to produce a general state diagram, including all the observed phenomena. Thus even if theoretical results do not reproduce a particular configuration examined in the experiments, the experimental observation with different amplifier and absorber conditions may be found within the presented state diagram. The parameters used in our numerical analysis of Eqs. (1) are presented in Table 1. The parameters corresponding to the SF_6 and $^{15}NH_3$ absorbers for LSA operating conditions near those of the reported unstable or

Table 1. Set of LSA Parameters

Parameter	Value
$2k$	1×10^{-7} sec^{-1}
B_{sg}/B_g	10^3
B_a/B_g	0.1–10^3
B_{sa}	$80\,B_a$
$R_{10}/2k$	0.2
$R_{20}/2k$	4×10^{-4}
$R_{21}/2k$	5×10^{-6}
$\gamma_R/2k$	8×10^{-2}
$\gamma'_R/2k$	4×10^{-5}
$\gamma_a/2k$	10^{-3}
$P/2k$	1–3×10^{-5}

chaotic regimes are close to those in Table 1. However, in the numerical analysis, smaller relaxation rates were used for the amplifier and absorber, corresponding to lower pressures, and a lower cavity loss was introduced corresponding to smaller output losses.

The LSA numerical analysis has been explored as a function of two control parameters: the pump parameter P, affecting the A parameter, and B_a, the absorption strength. Whereas in the experiment the P control parameter is modified through the discharge current, the B_a control parameter does not correspond directly to an experimentally accessible control parameter. A different B_a may be obtained by using different absorbers. The laser frequency used as a control parameter in the state diagram of Figs. 8 and 9 provides a limited tuning of the B_a absorption. However, the laser detuning also affects the pump parameter, so that a precise comparison between the experimental (A_0, Δ) and theoretical (P, B_a) state diagrams cannot be performed. The absorber pressure p is linearly proportional to B_{sa}, but it also affects the absorber relaxation rates except in the experiments at large buffer-gas pressure for which the absorber relaxation rates depend on the buffer pressure.

The numerically determined state diagram is given in Fig. 13, and Fig. 13(b) shows an enlargement of the framed area of 13(a). The diagram contains areas of off and cw operation and of bistability between off and cw operations (in the upper right-hand corner). The central part of the diagram contains an area of type-I and type-II instability regimes separated by chaotic regions or regions of period-doubling bifurcations on the type-I instabilities. The instability regions extend to the pointed area in the upper part of Fig. 13(b), but there the spacing between the different regions is too small to be resolved on the scale of the figure. For B_a intermediate values, which are scanning the P pump parameter, the chaotic regions are approached through direct or inverse cascades of period-doubling bifurcations. In the lower part of the diagram a small area of cw operation appears within the instability region. The heavy line passing near the top of Fig. 13(b) and delimiting from below the cw region in Fig. 13(a) is the line of the Hopf bifurcation. This line crosses the instability region and delimits, in the upper diagram, an area of bistability between cw and instability operations. As explained above, the regions of type-I instabilities are denoted by the index n of the homoclinic orbit or heteroclinic connection, and the regions of type-II instabilities are denoted as nT.

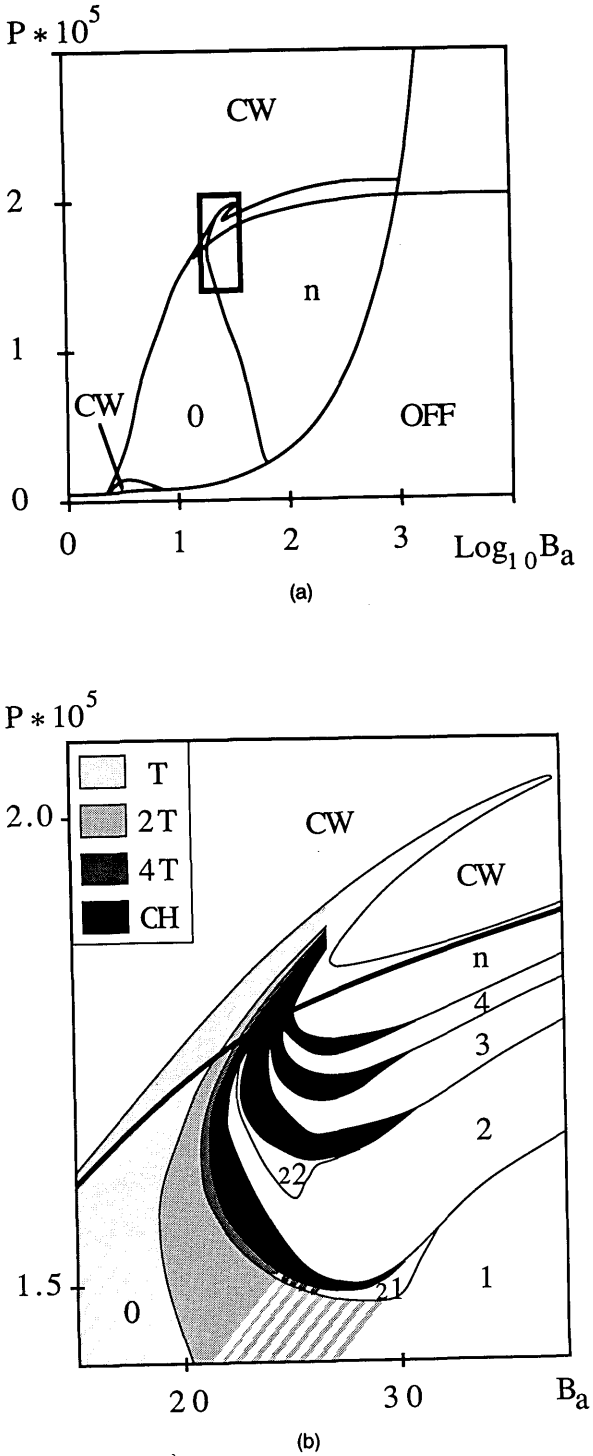

Fig. 13. Theoretical phase diagram of the LSA operation in the plane of the pump parameter P and the absorption coefficient B_a, both expressed in relative units, as presented in the text. (a) A general view of the phase diagram. (b) An expansion of the area shown in the box in (a). The bistable operation in the upper right-hand corner of (a) is between the cw and off regimes. The central area in (a) corresponds to the unstable regime, with the central line delimiting at the left where at low pump values $P^{(0)}$ instability occurs and a large pump value T instability occurs and at the right where $P^{(n)}$ and nT instabilities take place. Notice that between the Hopf bifurcation (heavy line) and the cw region an area exists in which bistability occurs between the cw and unstable regimes (either type I or type II).

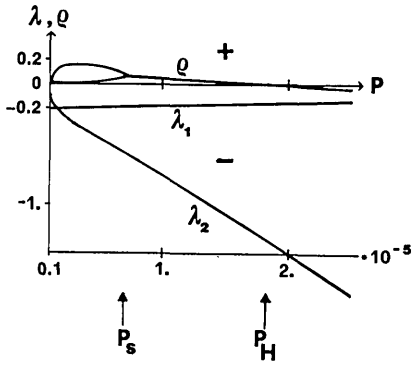

Fig. 14. Two real eigenvalues (λ_1 and λ_2) and the real part ρ of the complex-conjugate eigenvalues at the I_+ point for $B_a = 35$ as a function of the pump parameter P.

B. Eigenvalues

The LSA general behavior may be analyzed on the basis of the eigenvalues for the system of Eqs. (1) at the unstable I_0 and I_+ points. The I_0 point has four attractive eigenvalues, determined by the relaxation rates of the amplifier and absorber. The fifth eigenvalue, λ_0, is attractive at low pumping and is repulsive at large pumping, i.e., attractive whenever the $I = I_0$ solution is a stable one and repulsive when $I = I_0$ becomes an unstable saddle point. The I_+ point is a saddle focus in the instability region, with three real attractive eigenvalues and two complex ones $\{\lambda_i\ (i = 1, 3), \rho \pm i\omega\}$. The evolution of four relevant I_+ eigenvalues (expressed in units of $1/2k$) as a function of the pump parameter at a chosen B_a parameter and LSA parameters of Table 1 is shown in Fig. 14. The fifth attractive eigenvalue is large and does not depend significantly on P. For the conditions of Fig. 14, ω lies in the 10^{-1} range. In Fig. 14 the point P_s corresponds to a steady bifurcation point (bifurcation $I_0 - I_+$), P_H, to the Hopf bifurcation point ($\rho = 0$). The P_s point is also a bifurcation point for an infinite-period solution or homoclinic orbit at the I_0 point.[17] From Fig. 13(b) it appears that the instability region terminates at a P value larger than P_H, which cannot be resolved on the scale of Fig. 14. According to a theorem of Shil'nikov,[28] there exist infinitely many unstable periodic trajectories in systems that display a homoclinic orbit biasymptotic to a saddle focus, provided that $|\rho/\lambda| < 1$. The proximity of the Hopf bifurcation to the homoclinic bifurcation in LSA permits the Shil'nikov condition to be satisfied. However, in the LSA systems that we have explored theoretically and experimentally, two conditions are present to oppose the occurrence of Shil'nikov chaos, conceived as a large spread in the return times toward the saddle focus[18,19]: (i) homoclinic orbit biasymptotic to the I_+ saddle point does not occur in the typical conditions, (ii) the motion in the phase space is locally distorted by the presence of the I_0 stable point embedded within the flowing area of the I_+ point.

C. Phase-Space Orbits

Figure 15 shows the quite different trajectories on the phase space of three LSA variables (D, $\bar{D}$, I) for the $P^{(0)}$ and T instabilities. The I intensity is measured in units of $1/B_g$, and the I_0 point with coordinates (D_0, $\bar{D}_0$, 0) provides a reference scale for the amplifier and absorber population differences. In both cases the orbits take place near the I_+ point, but in the $P^{(0)}$ instability, during a large amount of the period T_p, the evolution takes place in the $I = I_0 = 0$ plane. Notice that the I_0 fixed point lies far from the phase-space trajectory; thus it is the invariant $I = I_0$ surface that plays a key role in determining the evolution of the trajectories in the $P^{(n)}$ instabilities, as already noted in Fig. 5. The trajectory evolves slowly when it is parallel to that surface before orbiting far into the phase space. Such behavior is produced by a motion within the strongly attractive I_0 manifold before reaching the I_0 repulsive direction. On the contrary, in the T instability the trajectory takes place near the I_+ point, and the I_0 point does not play any significant role. The trajectories of Fig. 15 give evidence for the large differences between the $P^{(0)}$ and T trajectories and more generally between the $P^{(n)}$ and nT trajectories. However, it is not possible to define a sharp transition between the two regimes. In fact, from the numerical point of view for the time evolution of the I intensity, the $P^{(0)}$ and T trajectories present only different orders of magnitude for the I variable

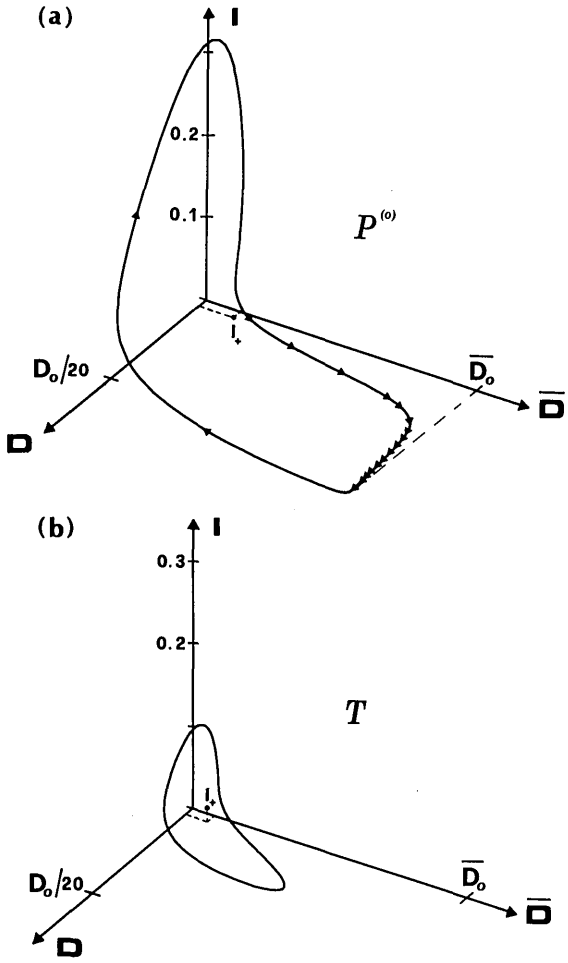

Fig. 15. Orbit in the three-dimensional phase space (D, $\bar{D}$, I) for $P^{(0)}$ and T instabilities in (a) and (b), with $P = 1 \times 10^{-5}$ and $P = 1.85 \times 10^{-5}$, respectively. $B_a = 25$, and the other parameters are as in Table 1. The I_0 point has coordinates (D_0, $\bar{D}_0$, 0). The arrows on the $P^{(0)}$ trajectory denote equally spaced times corresponding to a total $2kT_p = 180$.

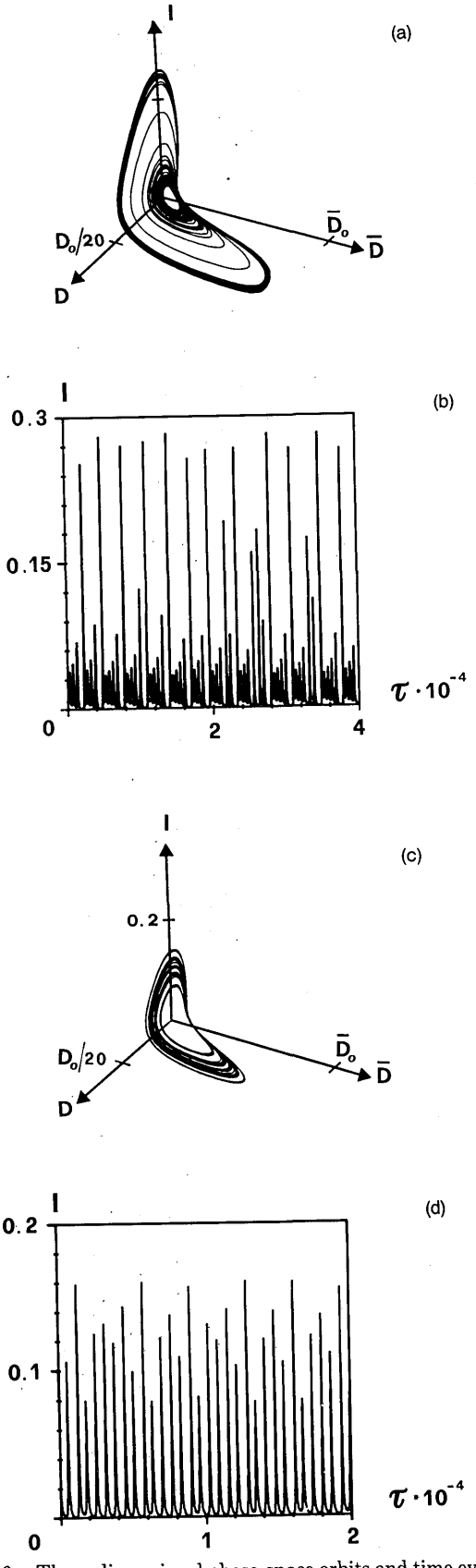

Fig. 16. Three-dimensional phase-space orbits and time evolution of the laser intensity I (versus reduced time $\tau = 2kt$) for chaotic motions. The LSA parameters are listed in Table 1 at $B_a = 25$ and $P = 1.76 \times 10^{-5}$ in (a) and (b) and $P = 1.832 \times 10^{-5}$ in (c) and (d).

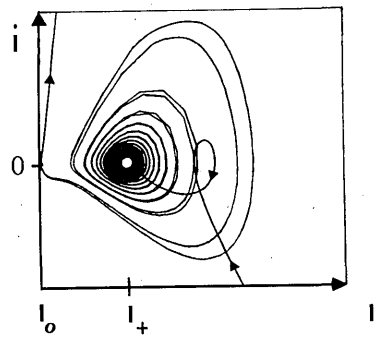

Fig. 17. Theoretical phase portrait $(I, \dot{I})$ around I_+ for a high n quasi-heteroclinic connection at $B_a = 40$ and $P = 1.85 \times 10^{-5}$, showing two successive trajectories evolving differently around I_+ but stabilized in passing through I_0.

but nothing qualitatively different. A type of distinction may be introduced if, for instance, we define as type-I trajectories those trajectories with I values less than $I_+/100$, but that distinction would be somewhat artificial. Thus the theoretical state diagram of Fig. 13 shows shaded areas for the transition between type-I and type-II instabilities.

Figure 16 shows phase-space orbits and time evolutions of the I intensity at the steady state in chaotic evolutions obtained in two different LSA conditions. For Figs. 16(a) and 16(b) chaos was reached starting with the $P^{(3)}$ evolution, and the attractor is spread on a narrow outside band and a broader one near I_+. For Figs. 16(c) and 16(d) chaos was reached from the $3T$ evolution, and the attractor contains a large central hole. Similar bands of chaotic attractors filled up ergodically have been investigated in the Belousov–Zhabotinskii reaction within nearly homoclinic conditions and analyzed by means of two- and one-dimensional Poincaré maps.[27] Such an approach will also be applied in the future to LSA in order to investigate the strange attractor more precisely.

Figure 17 shows part of a theoretical phase portrait in the $(I,\dot{I})$ space for a trajectory corresponding to a large-n-value, quasi-chaotic heteroclinic connection. Two successive orbits are presented. It appears that the two trajectories are returned to a small neighborhood of the I_+ saddle focus, and from there two quite different outward-spiraling evolutions take place. By expanding in the phase space, those orbits experience the I_0 attractive manifold and finally converge toward that point. Emerging from I_0, the two trajectories coalesce, and, in fact, a single trajectory appears returning to the I_+ saddle focus. Thus Fig. 17 gives clear evidence of the stability action exerted by the I_0 point on the complete trajectory. Even if small fluctuations in the I_+ reinjection lead to large variations in the orbit around that point, the passage near I_0 leads to a quite stable orbit in the large phase-space evolution.

5. CONCLUSION

The LSA unstable and chaotic regimes have been investigated as a function of the control parameters. In the experimental observations the phase portraits have been used to obtain a representation of the orbits in the phase space. The instabilities have been classified as type I (quasi-homo-

clinic orbits or quasi-heteroclinic connections) or type II, depending on the phase-space orbits. State diagrams showing the different operation regimes versus the control parameters have been derived. In the transitions between the different instability regimes, hesitations have been observed as characterized by large fluctuations produced by the noise influence on orbits that are sensitive to the initial conditions. In the transition regions the noise may mask the presence of microscopic chaos in a narrow region of control parameters.

In the experimental observations a richer behavior in the appearance of unstable and chaotic regimes was noticed whenever a high-pressure buffer gas was added to the absorber. The addition of the buffer gas allows us to operate the LSA in a regime of homogeneously broadened absorption line, but it is unlikely that the passage from an inhomogeneously to a homogeneously broadened regime enhances the occurrence of chaos. The addition of buffer gas modifies the rotational relaxation rates, proving the delicate balance of the LSA parameters required for the occurrence of chaos.

A numerical solution of the LSA equations has been used to investigate the unstable and chaotic regimes. Particular attention has been paid to the eigenvalue analysis. The parameters of the numerical simulation have been chosen in order to provide a varied behavior in the LSA state diagram. The LSA model includes the rotational coupling in the amplifier and absorber media. The inclusion of these rotational couplings does not modify the main features of the LSA chaotic behavior, which are produced by the internal dynamics in the pumping process of the CO_2 laser. However, the inclusion of the rotational coupling provides a proper fit of the static response and gives rise to a richer behavior in the LSA response.

Of particular concern in LSA behavior is the approach to chaos. We have observed chaotic regimes reached through a Feigenbaum scenario, i.e., sequences of period-doubling bifurcations in type-I and type-II instabilities. A possibility raised by the investigation of Dangoisse *et al.*[13] is the occurrence of Shil'nikov chaos in the LSA system. For the configurations investigated experimentally, as well as for the numerical solution, it appears that the LSA zero-intensity saddle point has a strong attractive force determining the evolution of the orbit in the phase space and eliminating the sensitivity to the initial conditions in the saddle focus. Therefore the Shil'nikov chaos cannot be realized. The main feature of the LSA theoretical analysis is probably the role played in the LSA global regime by the saddle point embedded in the flowing space around I_+. It would be important to explore whether there is any set of LSA parameters, still accessible to the experimental investigations, such that the I_0 point is not strongly attractive and where a Shil'nikov chaos would appear in the LSA operation.

In the bifurcation theory, in which small changes in certain parameters can lead to qualitative changes in the behavior of the solutions for the equations of the operating system, most of the attention is concentrated on the local nature. In addition to the local results, questions concerning the global behavior of the solutions, as well as the trajectories between critical points or how bifurcated solutions behave in general, are also relevant to describe the behavior of an operating system. In fact, we have shown that the LSA unstable regimes with large amplitude in the output power pulses are directly connected to trajectories between unstable points. For the present LSA problem it is relevant that the change of a control parameter, for instance, the pumping parameter A, splits apart the two unstable points I_0 and I_+, and new global phenomena appear out of the splitting. More precisely, trajectories joining these two points appear, and branches of periodic solutions terminating with finite-amplitude infinite-period solutions appear simultaneously. Most theoretical techniques for investigating the global behavior are topological, but analytical techniques for investigating, for instance, the trajectories between the critical points have also been developed. In close analogy with the recent study of chaotic relaxation oscillations in optically pumped molecular lasers,[29] it appears that much of the rich global dynamical behavior of the LSA remains to be discovered within a careful unfolding of higher-codimension bifurcations. Dangelmayr *et al.*[16] have analyzed codimension-three and -four bifurcations within the simplest model of two-level LSA. They presented some general phase portraits and bifurcation diagrams that included the results of the previous numerical analyses and are closely related to our instability observations. However, such an approach should be used on the LSA model, including the internal structure of the amplifier and absorber media.

ACKNOWLEDGMENTS

We wish to thank F. Tito Arecchi, Leone Fronzoni, and Pierre Glorieux for stimulating discussions. This research was performed within the Dynamics of Nonlinear Optical Systems Twinning Program of the European Economical Community. The research of Daniel Hennequin was supported by the European Economic Community through a visiting fellowship.

REFERENCES

1. For a review, see F. T. Arecchi and R. G. Harrison, eds., *Instabilities and Chaos in Quantum Optics* (Springer-Verlag, Berlin, 1987).
2. O. R. Wood and S. E. Schwarz, "Passive Q-switching of a CO_2 laser," Appl. Phys. Lett. **11**, 88–89 (1967).
3. I. Burak, P. L. Houston, D. G. Hutton, and J. I. Steinfeld, "Mechanism of passive Q switching in CO_2 lasers," IEEE J. Quantum Electron. **QE-17**, 73–82 (1971).
4. J. Dupré, F. Meyer, and C. Meyer, "Influence des phenomènes de relaxation sur la forme des impulsions fournies par un laser CO_2 déclenché par un absorbant saturable," Rev. Phys. Appl. **10**, 285–293 (1975); J. Dupré, *These de Doctorat d'Etat* (Université de Paris VI, Paris, 1975) (unpublished).
5. L. A. Lugiato, P. Mandel, S. T. Dembinski, and A. Kossakowski, "Semiclassical and quantum theories of bistabilities in lasers containing saturable absorbers," Phys. Rev. A **18**, 238–254 (1978).
6. E. Arimondo, F. Casagrande, L. Lugiato, and P. Glorieux, "Repetitive passive Q-switching and bistability in lasers with saturable absorber," Appl. Phys. B **30**, 57–77 (1983).
7. E. Arimondo, P. Bootz, P. Glorieux, and E. Menchi, "Pulse shape and phase diagram in the passive Q switching of CO_2 lasers," J. Opt. Soc. Am. B **2**, 193–201 (1985).
8. J. C. Antoranz, L. Gea, and M. G. Velarde, "Oscillatory phenomena and Q switching in a model for a laser with a saturable absorber," Phys. Rev. Lett. **47**, 1895–1898 (1981); M. G. Velarde and J. C. Antoranz, "Strange attractor (optical turbulence) in a model problem for the laser with saturable absorber and the

two-component Benard convection," Progr. Theor. Phys. **66,** 717–720 (1981); M. Velarde, "Benard convection and the laser with saturable absorber oscillations and chaos," in *Evolution of Order and Chaos in Physics, Chemistry and Biology*, H. Haken, ed. (Springer-Verlag, Berlin, 1982), pp. 132–145.

9. P. Mandel and T. Erneux, "Stationary, harmonic, and pulsed operations of an optically bistable laser with saturable absorber," Phys. Rev. A **30,** 1893–1901 (I), 1902–1909 (II) (1984); T. Erneux, P. Mandel, and J. F. Magnan, "Quasiperiodicity in lasers with saturable absorbers," Phys. Rev. A **29,** 2690–2699 (1986).
10. E. Arimondo, D. Dangoisse, and L. Fronzoni, "Transient bimodality in a bistable laser with saturable absorber," Europhys. Lett. **4,** 287–292 (1987).
11. E. Arimondo, D. Dangoisse, L. Fronzoni, O. Incani, and N. K. Rahman, "Optical bistability switching with external noise," AIP Conf. Proc. **160,** 190-195 (1987).
12. M. Tachikawa, K. Tanii, M. Kajita, and T. Shimizu, "Undamped undulation superposed on the passive Q-switching pulse of a CO_2 laser," Appl. Phys. B **39,** 83–90 (1986); "Comprehensive interpretation of passive Q switching and optical bistability in a CO_2 laser with an intracavity saturable absorber," J. Opt. Soc. Am. B **4,** 387–395 (1987).
13. D. Dangoisse, A. Bekkali, F. Papoff, and P. Glorieux, "Inverse Shil'nikov dynamics in a passive Q-switching laser," in *Digest of Instabilities, Dynamics, and Chaos in Nonlinear Optical Systems*, N. B. Abraham, E. Arimondo, and R. W. Boyd, eds. (ETS, Pisa, 1987); Europhys. Lett. **6,** 335–340 (1988).
14. D. Hennequin, F. de Tomasi, B. Zambon, and E. Arimondo, "Homoclinic orbits and cycles in the instabilities of a laser with saturable absorber," Phys. Rev. A **37,** 2243 (1988). Notice that in Fig. 4 a misprint occurred. The total time scale was 0.2 msec instead of 2 msec.
15. M. Tachikawa, F. Hong, K. Tanii, and T. Shimizu, "Determination of chaos in passive Q-switching pulsation of a CO_2 laser with saturable absorber," Phys. Rev. Lett. **60,** 2266–2268 (1988).
16. G. Dangelmayr, D. Ambruster, and M. Neveling, "A codimension three bifurcation for the laser with saturable absorber," Z. Phys. **59B,** 365–370 (1985); G. Dangelmayr, M. Neveling, and D. Ambruster, "Structurally stable phase portraits for the five-dimensional Lorenz equations," Z. Phys. **64B,** 491–501 (1986).
17. T. Erneux, "The Q-switching bifurcation in the laser with saturable absorber," J. Opt. Soc. Am. B **5,** 1063–1069 (1988).
18. F. T. Arecchi, R. Meucci, and K. Gadomski, "Laser dynamics with competing instabilities," Phys. Rev. Lett. **58,** 2205–2208 (1987).
19. F. T. Arecchi, R. Meucci, J. A. Roversi, and P. H. Coullet, "Experimental characterization of Shil'nikov chaos by statistics of return time," Europhys. Lett. **6,** 677–682 (1988).
20. B. Zambon, F. de Tomasi, D. Hennequin, and E. Arimondo, "A new model for the passive Q-switching in CO_2 lasers," in *Digest of Instabilities, Dynamics, and Chaos in Nonlinear Optical Systems*, N. B. Abraham, E. Arimondo, and R. W. Boyd, eds. (ETS, Pisa, 1987).
21. M. Tachikawa, M. Tanii, and T. Shimizu, "Laser instability and chaotic pulsation in CO_2 laser with intracavity saturable absorber," J. Opt. Soc. Am. B **5,** 1077–1082 (1988).
22. D. Dangoisse and P. Glorieux, "Feigenbaum and Shil'nikov chaos in a laser containing a saturable absorber: experiments and comparison with a simple theoretical model," to be submitted to J. Opt. Soc. Am. B.
23. K. Tanii, M. Tachikawa, M. Kajita, and T. Shimizu, "Sinusoidal self-modulation in the output of CO_2 laser with intracavity saturable absorber," J. Opt. Soc. Am. B **5,** 24–28 (1988).
24. E. Arimondo, D. Dangoisse, C. Gabbanini, E. Menchi, and F. Papoff, "Dynamic behavior of bistability in a laser with a saturable absorber," J. Opt. Soc. Am. B **4,** 892–899 (1987).
25. C. Salomon, *Thèse de Docteur de troisième cycle* (Université de Paris-Nord, Paris, 1979) (unpublished); C. Bréant, *Thèse de Docteur es Sciences* (Université de Paris-Nord, Paris, 1985) (unpublished).
26. J. Guckenheimer and P. Holmes, *Nonlinear Oscillations, Dynamical Systems and Bifurcation of Vector Fields* (Springer-Verlag, Berlin, 1984).
27. F. Argoul, A. Arneodo, P. Richetti, and J. C. Roux, "Experimental evidence for homoclinic chaos in the Belousov–Zhabotinski reaction," J. Chem. Phys. **86,** 3325 (1987).
28. L. P. Shil'nikov, "A case of the existence of a denumerable set of periodic motions," Sov. Math. Dokl. **6,** 163–166 (1965).
29. J. V. Moloney, J. S. Uppal, and R. G. Harrison, "Origin of chaotic relaxation oscillations in an optically pumped molecular laser," Phys. Rev. Lett. **59,** 2868–2871 (1987).